racarboxylic acid (**8**) (141 g) directly in 91% yield, which is an important intermediate for synthetic resins and flexibilizers. Cyclohexene-*cis*-4,5-dicarboxylic acid was also convertible to **8** in 96% yield (*17*). Under standard conditions, 1-methylcyclohexene was converted to 6-oxoheptanoic acid (**9**) in 59% yield. Oxidation of cyclopentene (100 g) with 30% H_2O_2 (736 g), $Na_2WO_4 \cdot 2H_2O$ (4.84 g), and $[CH_3(n\text{-}C_8H_{17})_3N]HSO_4$ (6.84 g) at 70° to 90°C for 13 hours produced crystalline glutaric acid (**10**) (175 g) in 90% yield. Oxidative cleavage of the C(9)–C(10) bond of phenanthrene with the aid of (aminomethyl)phosphonic acid (*7*) produced 2,2′-biphenyldicarboxylic acid (**11**) in 41% yield. Cyclooctene and 1-octene produced suberic acid and heptanoic acid in only 9 and 36% yield, respectively, because the initially formed epoxides are resistant to hydrolytic cleavage.

This solvent- and halide-free oxidation of cyclohexene and cyclopentene is clean, safe, and reproducible, with conditions that are less corrosive than those of the nitric acid oxidation. No operational problems are foreseen for a large-scale version of this "green" process, and technical refinement should further increase the synthetic efficiency. The worldwide chemical industry is directing extensive efforts toward the efficient production of H_2O_2 as a clean, selective oxidant (*18*). Thus, this environmentally conscious, non–nitric acid route to adipic acids will be attractive only if the cost of H_2O_2 is considerably reduced or if the regulations regarding N_2O emission become more stringent.

References and Notes

1. D. D. Davis and D. R. Kemp, in *Kirk-Othmer Encyclopedia of Chemical Technology*, J. I. Kroschwitz and M. Howe-Grant, Eds. (Wiley, New York, 1991), vol. 1, pp. 466–493.
2. M. H. Thiemens and W. C. Trogler, *Science* **251**, 932 (1991).
3. A. Scott, *Chem. Week* **160** (no. 6) 37 (1998); R. A. Reimer, C. S. Slaten, M. Seapan, M. W. Lower, P. E. Tomlinson, *Environ. Prog.* **13**, 134 (1994).
4. R. E. Dickinson and R. J. Cicerone, *Nature* **319**, 109 (1986).
5. For synthesis from D-glucose, see K. M. Draths and J. W. Frost, *J. Am. Chem. Soc.* **116**, 399 (1994).
6. For international regulations, see Regulations Concerning the International Carriage of Dangerous Goods by Rail (RID), European Agreement Concerning the International Carriage of Dangerous Goods by Road (ADR), International Maritime Dangerous Goods Code (IMDG Code), International Civil Aviation Organization Technical Instructions for the Safe Transport of Dangerous Goods by Air (ICAO TI), and International Air Transport Association Dangerous Goods Regulation (IATA DGR).
7. K. Sato, M. Aoki, M. Ogawa, T. Hashimoto, R. Noyori, *J. Org. Chem.* **61**, 8310 (1996); K. Sato *et al.*, *Bull. Chem. Soc. Jpn.* **70**, 905 (1997).
8. K. Sato, M. Aoki, J. Takagi, R. Noyori, *J. Am. Chem. Soc.* **119**, 12386 (1997).
9. For nonacidic epoxidation with aqueous H_2O_2, see J. Rudolph, K. L. Reddy, J. P. Chiang, K. B. Sharpless, *ibid.*, p. 6189; C. Copéret, H. Adolfsson, K. B. Sharpless, *Chem. Commun.* **1997**, 1565 (1997).
10. Cyclohexene is produced by the hydrogenation of benzene for the industrial preparation of **1**; see O. Mitsui and Y. Fukuoka, Japanese Patents 59-184138 and 59-186929 (1984); H. Nagahara and Y. Fukuoka, *ibid.* 61-50930 (1986); H. Nagahara and M. Konishi, *ibid.* 62-45541 (1987).
11. The typical procedure of oxidation and reuse of the water phase are given as follows. In the first run, a 1-liter round-bottomed flask equipped with a magnetic stirring bar and a reflux condenser was charged with 4.01 g (12.2 mmol) of $Na_2WO_4 \cdot 2H_2O$, 5.67 g (12.2 mmol) of $[CH_3(n\text{-}C_8H_{17})_3N]HSO_4$, and 607 g (5.355 mol) of aqueous 30% H_2O_2. The mixture was vigorously stirred at room temperature for 10 min and then 100 g (1.217 mol) of **1** was added. The biphasic mixture was heated successively at 75°C for 30 min, at 80°C for 30 min, at 85°C for 30 min, and at 90°C for 6.5 hours, with stirring at 1000 rpm. The homogeneous solution was allowed to stand at 0°C for 12 hours, and the resulting white precipitate was separated by filtration and washed with 20 ml of cold water. The product was dried in a vacuum to produce 138 g (78% yield) of **2** as a white solid (with a melting point of 151.0° to 152.0°C). A satisfactory elemental analysis was obtained without further purification. Concentration of the mother liquor produced 23 g of pure **2**; the yield determined by GC (OV-1 column, 0.25 mm by 50 m, GL Sciences, Tokyo) was 93%. The identified byproducts were 1,2-cyclohexanediol (2% yield) and glutaric acid (4% yield). In the second run, a 2-liter round-bottomed flask was charged with the water phase of the first run, which contained the W catalyst, 5.67 g (12.2 mmol) of $[CH_3(n\text{-}C_8H_{17})_3N]HSO_4$, and 552 g (4.868 mol) of aqueous 30% H_2O_2. After the mixture was vigorously stirred at room temperature for 10 min, 100 g (1.217 mol) of **1** was added. This mixture was heated successively at 75°C for 30 min, at 80°C for 30 min, at 85°C for 30 min, and at 90°C for 46.5 hours, with stirring at 1000 rpm; the homogeneous solution was allowed to stand at 0°C for 12 hours. The resulting white precipitate was separated, washed, and dried in a vacuum to produce 138 g (78% yield) of analytically pure **2** as a white solid.
12. Y. Ishii *et al.*, *J. Org. Chem.* **53**, 3587 (1988); T. Oguchi, T. Ura, Y. Ishii, M. Ogawa, *Chem. Lett.* **1989**, 857 (1989).
13. C. Venturello and M. Ricci, European Patent 0 122 804 (1984).
14. T. Fujitani and M. Nakazawa, Japanese Patent 63-93746 (1988). An experiment that we conducted under the reported conditions produced a 61% yield of **2** that was contaminated with glutaric acid (5% yield), peroxy acids (5% yield), and 1,2-cyclohexanediol (3% yield). With 35% H_2O_2 and a H_2WO_4 catalyst, only a trace amount of **2** was obtained (*12*).
15. L. Knof, *Liebigs Ann. Chem.* **656**, 183 (1962); G. M. Rubottom, J. M. Gruber, R. K. Boeckman Jr., M. Ramaiah, J. B. Medwid, *Tetrahedron Lett.* **1978**, 4603 (1978).
16. Under the standard conditions of alcohol oxidation, Baeyer-Villiger ring enlargement of simple cyclohexanones is negligible (*8*). A separate experiment showed that 1,2-cyclohexanedione is not a reaction intermediate.
17. For nitric acid oxidation, see J. E. Franz, J. F. Herber, W. S. Knowles, *J. Org. Chem.* **30**, 1488 (1965).
18. *Eur. Chem. News* **66**, 41 (1996); L. W. Gosser, U.S. Patent 4,681,751 (1987).

19. We are grateful to N. Imaki and T. Setoyama (Mitsubishi Chemical Company, Tokyo), M. Kagotani (Daicel Chemical Industries, Osaka), T. Kurai (Mitsubishi Gas Chemical Company, Tokyo), M. Minai (Sumitomo Chemical Industry, Tokyo), and K. Nakagawa (Asahi Chemical Industry Company, Tokyo) for their valuable comments from industrial points of view. This work was supported by the Ministry of Education, Science, Sports, and Culture, Japan (grant 07CE2004).

2 June 1998; accepted 23 July 1998

Onset of Catalytic Activity of Gold Clusters on Titania with the Appearance of Nonmetallic Properties

M. Valden,* X. Lai, D. W. Goodman†

Gold clusters ranging in diameter from 1 to 6 nanometers have been prepared on single crystalline surfaces of titania in ultrahigh vacuum to investigate the unusual size dependence of the low-temperature catalytic oxidation of carbon monoxide. Scanning tunneling microscopy/spectroscopy (STM/STS) and elevated pressure reaction kinetics measurements show that the structure sensitivity of this reaction on gold clusters supported on titania is related to a quantum size effect with respect to the thickness of the gold islands; islands with two layers of gold are most effective for catalyzing the oxidation of carbon monoxide. These results suggest that supported clusters, in general, may have unusual catalytic properties as one dimension of the cluster becomes smaller than three atomic spacings.

An atomic-level understanding of structure-activity relations in surface-catalyzed reactions is one of the most important goals of surface science studies related to heterogeneous catalysis. Planar model catalysts (*1*–*3*) consisting of metal clusters supported on thin (2.0 to 10 nm) oxide films simulate the critical features of most practical high surface area metal catalysts, yet are tractable for a wide range of surface analytical probes. The oxide films (SiO_2, Al_2O_3, TiO_2, MgO) used are thin enough to be suitably conductive for use with various electron spectroscopies in-

Department of Chemistry, Texas A&M University, College Station, TX 77842–3012, USA.

*Visiting Scientist, Department of Physics, Tampere University of Technology, Tampere, FIN 33101, Finland.
†To whom correspondence should be addressed: E-mail: goodman@chemvx.tamu.edu

cluding STM and STS.

We have used such model catalysts to study the unusual and as yet unexplained catalytic properties of nanosize Au clusters. STM, STS, and elevated pressure reaction kinetics measurements demonstrate that the structure sensitivity of the CO oxidation reaction on Au clusters supported on TiO_2 is related to a quantum size effect with respect to the thickness of the Au clusters; clusters with a two-layer thickness of Au, which exhibit a band gap uncharacteristic of bulk metals, are shown to be particularly suited for catalyzing the oxidation of CO.

Gold has long been known as being catalytically far less active than other transition metals. Quite recently, however, it was found that when dispersed as ultrafine particles and supported on metal oxides such as TiO_2, Au exhibits an extraordinary high activity for low-temperature catalytic combustion, partial oxidation of hydrocarbons, hydrogenation of unsaturated hydrocarbons, and reduction of nitrogen oxides (*4*). For example, Au clusters can promote the reaction between CO and O_2 to form CO_2 at temperatures as low as 40 K (*5*). The catalytic properties of Au depend on the support, the preparation method, and particularly the size of the Au clusters. The structure sensitivity of the low-temperature oxidation of CO on supported Au clusters manifests as a marked increase in the reaction rate per surface Au site per second, or turnover frequency, as the diameter of the Au clusters is decreased below ~3.5 nm (*6*, *7*) (Fig. 1). A further decrease in cluster diameter below ~3 nm leads to a decrease in the activity of the Au. Despite the extensive recent efforts addressing this extraordinary catalytic behavior, no atomic-level understanding currently exists.

Constant current topographic (CCT) images were obtained by applying a positive bias voltage of 2.0 V to the sample with a tunneling current of 2.0 nA. Figure 2A shows a CCT STM image of 0.25 monolayers (ML) Au on $TiO_2(110)$-(1×1) after deposition of Au at 300 K and annealing at 850 K for 2 min (*8*, *9*). The $TiO_2(110)$ surface consists of flat (1×1) terraces separated by monoatomic steps. Recently, it was shown that Ti cations instead of O anions are generally imaged in STM (*9*). Individual atom rows separated by ~0.65 nm can also be resolved on the terraces corresponding to the length of the unit cell along the [1$\bar{1}$0] direction of the unreconstructed $TiO_2(110)$-(1×1) surface. The Au clusters are imaged as bright protrusions with a relatively narrow size distribution. The clusters, with an average size of ~2.6 nm in diameter and ~0.7 nm in height (two to three atomic layers), preferentially nucleate on the step edges of the $TiO_2(110)$-(1×1) substrate. By varying the initial Au coverage, clusters from 1 to 50 nm can be synthesized with relatively narrow cluster size distributions (*9*, *10*).

STS spectra were recorded during the CCT imaging by stopping the scan at a certain point of interest, interrupting the STM feedback loop, and measuring the tunneling current (I) as a function of the bias voltage (V). These I-V curves can then be correlated with the corresponding geometric features on the surface. Figure 2B shows STS data acquired for the bare $TiO_2(110)$-(1×1) surface and for overlying Au clusters of varying sizes.

To address the basic issues relating to the structure sensitivity of CO oxidation over supported Au catalysts, we investigated the reaction of CO and O_2 on Au clusters of varying size supported on $TiO_2(110)$-(1×1) at reaction conditions similar to those used in actual technological applications and in (*6*).

The reaction studies of this surface indeed show a marked size effect of the catalytic activity of the supported Au clusters for the CO oxidation reaction, with Au clusters in the range of 3.5 nm exhibiting the maximum reactivity (Fig. 3A).

The I-V characteristics obtained from sev-

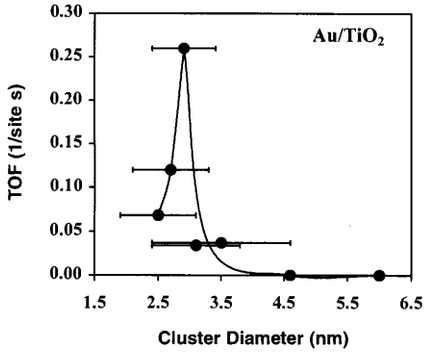

Fig. 1. CO oxidation turnover frequencies (TOFs) at 300 K as a function of the average size of the Au clusters supported on a high surface area TiO_2 support (*7*). The Au/TiO_2 catalysts were prepared by deposition-precipitation method, and the average cluster diameters were measured by TEM. The solid line serves merely to guide the eye.

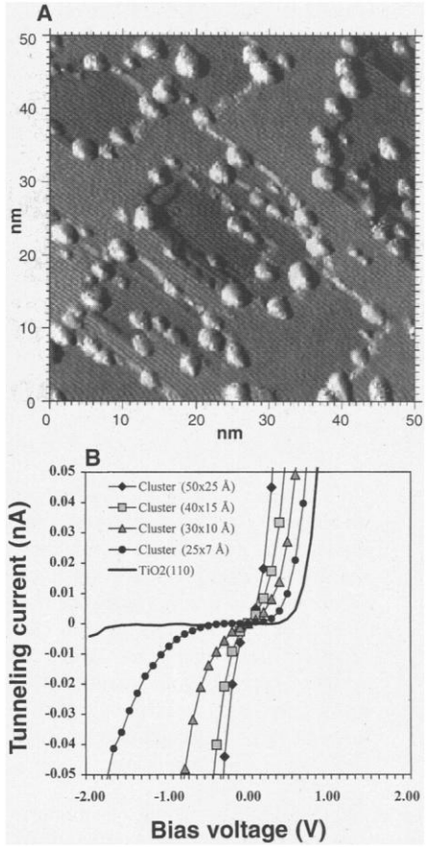

Fig. 2. (**A**) A CCT STM image of Au/$TiO_2(110)$-(1×1) as prepared before a CO:O_2 reaction. The Au coverage is 0.25 ML, and the sample was annealed at 850 K for 2 min. The size of the images is 50 nm by 50 nm. (**B**) STS data acquired for Au clusters of varying sizes on the $TiO_2(110)$-(1×1) surface. For reference, the STS of the $TiO_2(110)$-(1×1) substrate is also shown.

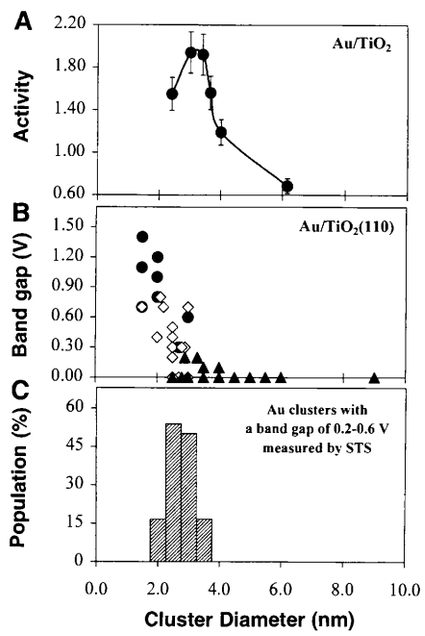

Fig. 3. (**A**) The activity for CO oxidation at 350 K as a function of the Au cluster size supported on $TiO_2(110)$-(1×1) assuming total dispersion of the Au. The CO:O_2 mixture was 1:5 at a total pressure of 40 Torr. Activity is expressed as (product molecules) × (total Au atoms)$^{-1}$ s^{-1}. (**B**) Cluster band gap measured by STS as a function of the Au cluster size supported on $TiO_2(110)$-(1×1). The band gaps were obtained while the corresponding topographic scan was acquired on various Au coverages ranging from 0.2 to 4.0 ML. (●) Two-dimensional (2D) clusters; (□) 3D clusters, two atom layers in height; (▲) 3D clusters with three atom layers or greater in height. (**C**) Relative population of the Au clusters (two atom layers in height) that exhibited a band gap of 0.2 to 0.6 V as measured by STS from Au/$TiO_2(110)$.

eral Au clusters supported on TiO_2(110)-(1×1) for various Au coverages from 0.2 to 4.0 ML are shown in Fig. 3B in terms of their band gaps as a function of the Au cluster size. A metal-to-nonmetal transition occurs as the cluster size is decreased below 3.5 by 1.0 nm^2 (3.5 nm in diameter and 1.0 nm in height, ~300 atoms per cluster). This result is similar to that of Pd/TiO_2(110) for which the metal-to-nonmetal transition occurs at a cluster size of 3.0 nm by 1.1 nm (~300 atoms per cluster) (*9*).

The relative population of the Au clusters with a band gap of 0.2 to 0.6 V measured by STS from Au/TiO_2(110) is shown in Fig. 3C. This band gap is associated primarily with those Au clusters whose thickness corresponds to that of two Au atoms. Clusters that are only one atom thick have band gaps significantly larger, whereas clusters with thicknesses of three atoms or greater exhibit metallic properties. The population of two-atom-thick clusters is clearly peaked at diameters ranging from 2.5 to 3.0 nm, which coincides with the maximum of the specific activity of the model and high-area Au/TiO_2 catalysts (Figs. 1 and 3A).

A series of CCT STM images of the TiO_2(110)-(1×1) surface of Fig. 2 show the effect of separate 120-min exposures of CO, O_2, and CO:O_2 (2:1), respectively, at a total pressure of 10 Torr in the sealed reactor chamber and at 300 K. The CO exposure has no effect on the morphology of the Au/TiO_2(110)-(1×1) surface, whereas significant changes occur after exposure to O_2 or CO:O_2 (Fig. 4, A and B). In the latter exposures, the Au cluster density was greatly reduced as a result of sintering to form much larger clusters with an average diameter and height of ~3.6 and ~1.4 nm, respectively. In addition to the significant agglomeration of the Au clusters, extremely small, presumably TiO_2 clusters (~1.5 nm in diameter), were formed. X-ray photoemission spectra (XPS) before and after the CO exposure show no changes in the chemical composition of the Au/TiO_2(110)-(1×1) surface; however, the TiO_2(110) surface oxidized after the CO:O_2 (and O_2 alone, not shown) exposure (Fig. 5). A small shoulder at the low binding energy side of the XPS Ti 2*p* transition, owing to the presence of Ti^{3+} species, was completely absent after the 120-min CO:O_2 exposure at 300 K. Because all of the structural and surface chemical changes upon exposure to O_2 and CO:O_2 were identical and because there were no detectable changes after exposure to CO, we conclude that the Au/TiO_2(110) surface exhibits an exceptionally high reactivity toward O_2 at 300 K that promotes the sintering of the Au nanocrystallites. The possible effect of thermal sintering can be excluded because of the anneal to 850 K before the adsorption experiments. Although O_2 adsorption on atomically flat metal single crystals of Au is a highly activated process with an extremely low sticking probability at 300 K (*11*), Au nanoclusters can activate O_2 and produce atomically adsorbed O atoms on Au clusters (*12*).

In the reaction kinetics studies (discussed above), the Au clusters exhibited a very high activity toward CO oxidation; however, the surface was effectively deactivated after reaction for 120 min. This deactivation is believed to be caused by O_2-induced agglomeration of the Au clusters as seen in Fig. 4B. The oxidation of the slightly oxygen-defi-

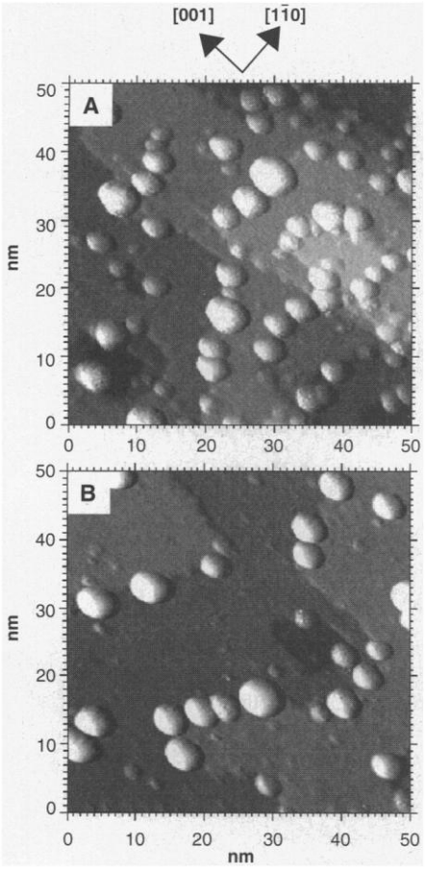

Fig. 4. A series of CCT STM images of Au/TiO_2(110)-(1×1) as prepared in Fig. 2 (**A**) after 120 min of O_2 exposure at 10 Torr, and (**B**) after 120 min of CO:O_2 (2:1) exposure at 10 Torr. The Au coverage was 0.25 ML, and the sample was annealed at 850 K for 2 min before the exposures. All of the exposures are given at 300 K. The size of the images is 50 nm by 50 nm.

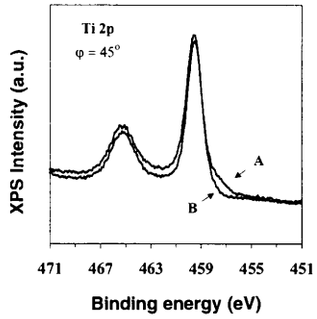

Fig. 5. Core-level spectra (Ti 2*p*) of Au/TiO_2(110)-(1×1) measured at grazing emission, φ = 45° off the crystal normal, (**A**) before CO:O_2 exposure and (**B**) after 120 min of CO:O_2 exposure at 10 Torr and 300 K. The Au coverage was 0.25 ML and the sample was annealed at 850 K for 2 min before the CO:O_2 exposure.

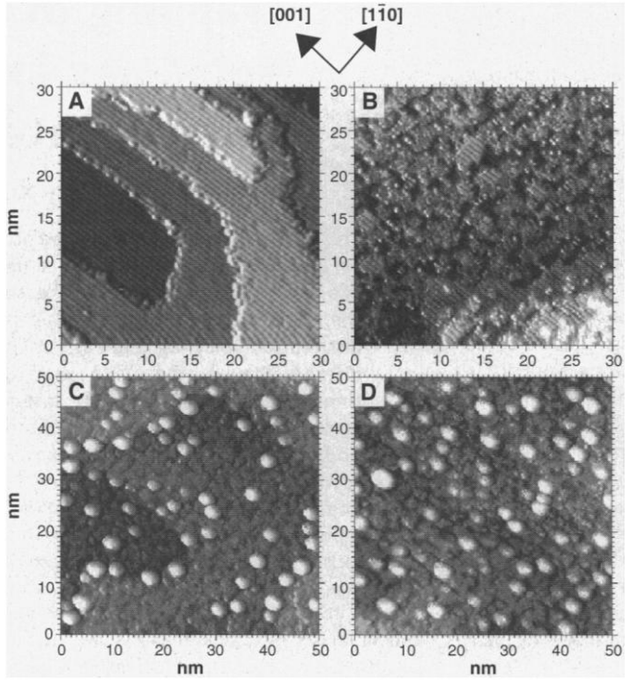

Fig. 6. Two CCT STM images of TiO_2(110)-(1×1). (**A**) Clean surface, before O_2 exposure, and (**B**) after a 12-L exposure of O_2 at 650 K (1 L = 10^{-6} Torr-s). The size of the images is 30 nm by 30 nm. Two CCT STM images of Au/TiO_2(110)-(1×1). (**C**) Before CO:O_2 exposure, and (**D**) after 120 min of CO:O_2 (2:1) exposure at 10 Torr and 300 K. The Au coverage was 0.25 ML and the sample was exposed to 2 × 10^{-8} Torr of O_2 at 650 K for 10 min (~12 L) before the exposures. Image sizes are 50 nm by 50 nm.

cient TiO_2 surface after the 120-min CO:O_2 exposure (Fig. 5) is likely lowering the activity of Au/TiO_2 even further, because the fully oxidized stoichiometric TiO_2 surface can no longer adsorb O_2 at 300 K (*13*). Oxidation of the TiO_2 surface during CO oxidation also provides direct evidence that the deactivation is not likely caused by encapsulation of Au clusters by reduced Ti suboxides as, for example, in the case of Pt/TiO_2(110) (*14*).

In order to better understand the role of O_2 in CO oxidation and in various O_2 pretreatments that are commonly applied to Au/TiO_2 catalysts to improve their activity (*15*), the clean TiO_2(110) surface (Fig. 6A) was exposed to O_2 at 2×10^{-8} Torr. After O_2 treatment, small islands randomly nucleated on TiO_2(110) and finally covered the entire surface (Fig. 6B). Low-energy electron diffraction (LEED) showed a (1×1) pattern indicating that the islands are growing pseudomorphically. XPS measurements of this rough TiO_2 surface after the O_2 treatment indicate that the surface is not significantly changed in chemical composition and thus is still slightly O-deficient. Recently, it was suggested that partially reduced Ti^{n+} ($n \leq 3$) ions can be formed in a vacuum-annealed and Ar^+-bombarded TiO_2(110) surface by annealing at 800 K and reoxidizing to TiO_2(110)-(1×1) terraces in an O_2 ambient of 7.5×10^{-8} Torr (*7*). A similar kind of oxidation of the reduced Ti^{n+} ions may occur during the O_2 treatment used here.

The influence of the O_2-exposed, rough TiO_2 surface on the sintering of the Au clusters during CO oxidation at 300 K is shown in Fig. 6, C and D. If we compare a CCT STM image of 0.25 ML Au on TiO_2(110)-(1×1) after deposition of Au at 300 K, annealing at 850 K for 2 min, and a subsequent O_2 exposure of 2×10^{-8} Torr at 650 K for 10 min (Fig. 6C) with one for which no O_2 treatment was made (Fig. 2A), the only difference is the general disorder of the TiO_2 surface. The cluster density and size distribution of the Au clusters are identical for both surfaces. Upon exposure of the rough Au/TiO_2(110) surface to CO:O_2 for 120 min at a total pressure of 10 Torr at 300 K, the cluster density and size distribution of the Au clusters remain unchanged (Fig. 6D). The Au/TiO_2(110) surface was oxidized after the high pressure CO:O_2 exposure (Fig. 4) and the cluster density of the TiO_2 clusters increased. The O_2-exposed, rough TiO_2 surface then prevents sintering of the Au clusters. Furthermore, a similar kind of atomically rough TiO_2 phase may be formed during the high-temperature reduction, calcination, and low-temperature reduction (HTR/C/LTR) procedure used on high–surface area Au/TiO_2 catalysts (*15*). After this treatment Au/TiO_2 catalysts exhibit a higher degree of resistance toward sintering of the Au clusters during CO oxidation at low temperatures (*15*).

These results indicate that the pronounced structure sensitivity of CO oxidation on Au/TiO_2 originates from quantum size effects associated with the supported Au clusters. The observed tailoring of the properties of small metal clusters by altering the cluster size and its support could prove to be universal for a variety of metals and will likely be quite useful in the design of nanostructured materials for catalytic applications.

References and Notes

1. D. R. Rainer, C. Xu, D. W. Goodman, *J. Mol. Catal. A Chem.* **119**, 307 (1997).
2. S. C. Street and D. W. Goodman, *The Chemical Physics of Solid Surfaces*, D. A. King and D. P. Woodruff, Eds. (Elsevier, Amsterdam, 1997), vol. 8, p. 375.
3. D. W. Goodman, *J. Phys. Chem. (Centennial Ed.)* **100**, 13090 (1996).
4. M. Haruta, *Catal. Catal. Today* **36**, 153 (1997).
5. H. Huber, D. McIntosh, G. A. Ozin, *Inorg. Chem.* **16**, 975 (1977).
6. M. Haruta *et al.*, *J. Catal.* **144**, 175 (1993).
7. G. R. Bamwenda, S. Tsubota, T. Nakamura, M. Haruta, *Catal. Lett.* **44**, 83 (1997).
8. The experiments were carried out in a combined elevated-pressure reactor–ultrahigh vacuum (UHV) system with a base pressure of 5×10^{-11} Torr equipped with a double-pass cylindrical mirror analyzer for Auger electron spectroscopy (AES) and XPS measurements, a quadrupole mass analyzer, and a UHV-STM (Omicron) [R. A. Campbell and D. W. Goodman, *Rev. Sci. Instrum.* **63**, 172 (1992)]. After preparation and characterization in the UHV chamber, the Au/TiO_2(110) model catalyst was transferred in situ into the reaction chamber through a double-stage, differentially pumped Teflon sliding seal. This arrangement facilitates elevated-pressure adsorption studies in the pressure range of 1×10^{-8} to 1×10^{3} Torr. A TiO_2(110) single crystal (Commercial Crystal Laboratories), an *n*-type semiconductor after cycles of Ar^+-ion bombardment and vacuum annealing at 700 to 1100 K, was found to be sufficiently conductive for electron spectroscopy and STM studies. This cleaning procedure produces a slightly oxygen-deficient surface with a well-ordered (1×1) surface as characterized by LEED and XPS measurements [J.-M. Pan, B. L. Maschhoff, U. Diebold, T. E. Madey, *J. Vac. Sci. Technol. A* **10**, 2470 (1992); L. Zhang, R. Persaud, T. E. Madey, *Phys. Rev. B* **56**, 10549 (1997)]. Gold clusters were evaporated onto the TiO_2(110) surface from a source containing high-purity Au wire wrapped around a W filament that was heated resistively. The Au flux was calibrated with a Re(0001) subtrate by using AES and STM as described (*13*). The Au coverage is reported in monolayers (ML), one ML corresponding to 1.387×10^{15} atoms per centimeter squared. After the Au deposition, the sample was annealed at 850 K for 2 min. The sample temperature was measured with a pyrometer (OMEGA OS3700), which was calibrated against a W-5% Re/W-26% Re thermocouple. Research-grade CO was further purified by storing at liquid N_2 temperatures; O_2 was used as received. The CO:O_2 (2:1) mixture was prepared separately before the adsorption experiments.
9. C. Xu, X. Lai, G. W. Zajac, D. W. Goodman, *Phys. Rev. B* **56**, 13464 (1997).
10. S. Pak, M. Valden, X. Lai, D. W. Goodman, in preparation.
11. N. D. S. Canning, D. Outka, R. J. Madix, *Surfactant Sci.* **141**, 240 (1984).
12. Y. Iizuka *et al.*, *Catal. Today* **36**, 115 (1997).
13. C. Xu, W. S. Oh, G. Liu, D. Y. Kim, D. W. Goodman, *J. Vac. Sci. Technol. A* **15**, 1261 (1997).
14. F. Pesty, H.-P. Steinrück, T. E. Madey, *Surfactant Sci.* **339**, 83 (1995).
15. S. D. Lin, M. Bollinger, M. A. Vannice, *Catal. Lett.* **17**, 245 (1993).

16. We acknowledge the support of this work by the Department of Energy, Office of Basic Energy Sciences, Division of Chemical Sciences, the Robert A. Welch Foundation, and the Dow Chemical Company. M.V. thanks the Academy of Finland for support as a Visiting Scientist.

7 May 1998; accepted 31 July 1998

Long-Range Electrostatic Trapping of Single-Protein Molecules at a Liquid-Solid Interface

Xiao-Hong Nancy Xu* and Edward S. Yeung†

The motion of single, dye-labeled protein molecules was monitored at various pH and ionic strengths within the 180-nanometer-thick evanescent-field layer at a fused-silica surface. Below the isoelectric point, molecules partitioning into the excitation region increased in number but maintained a random spatial distribution, implying that surface charge can influence the charged protein at distances beyond that of the electrical double-layer thickness. The residence times of the molecules in the interfacial layer also increased below the isoelectric point. However, immobilization on the solid surface for extended periods was not observed. Histograms of residence times exhibit nearly identical asymmetry as the corresponding elution peaks in capillary electrophoresis. These results are a direct verification of the statistical theory of chromatography at the single-molecule level, with the caveat that long-range trapping rather than adsorption is the dominant mechanism.

Insights into the detailed dynamics of adsorption and desorption at an interface are vital to designing new materials, elucidating biological processes at cell surfaces, studying electrochemical reactions, and understanding chromatographic mechanisms. For example,